Appendix to:

NDST3 Deacetylates α-tubulin and Suppresses V-ATPase Assembly and Lysosomal Acidification

Table of Contents

Appendix Table S1. List of patients' B lymphocytes and spinal cord tissues (related to Fig 6)

Sample No.	Patient ID	Source	Clinical diagnosis	ALS pathology	Age of sampling	Gender	Sample Type
B6	ND03053 C	Coriell	CTRL	Non	69	F	B-LYM
B10	ND09374 A	Coriell	CTRL	Non	59	F	B-LYM
B11	ND11549 A	Coriell	CTRL	Non	67	F	B-LYM
B7	ND10123 A	Coriell	ALS-C9orf72	Yes	56	M	B-LYM
B1	ND06769 B	Coriell	ALS-C9orf72	Yes	46	F	B-LYM
B3	ND08544 A	Coriell	ALS-C9orf72	Yes	61	F	B-LYM
#1	95	JHMI	CTRL	Non	72	M	SC-C
#2	120016	VABBB	CTRL	Non	63	F	SC-C
#3	90018	VABBB	CTRL	Non	82	M	SC-C
#4	100012	VABBB	CTRL	Non	81	F	SC-C
#I	38	JHMI	sALS-C9orf72	Yes	34	F	SC-C
#II	88	JHMI	fALS-C9orf72	Yes	59	M	SC-C
#III	NEUTP019MY9	BNI	ALS-C9orf72	Yes	62	F	SC-C
#IV	92	JHMI	fALS-C9orf72	Yes	72	M	SC-C
#V	10007	VABBB	fALS-C9orf72	Yes	61	M	SC-C

Note: ALS, Amyotrophic Lateral Sclerosis; B-LYM, B Lymphocytes; BNI, Barrow Neurological Institute; CTRL, Control; F, Female; fALS, Familial Amyotrophic Lateral Sclerosis; FTD, Frontotemporal Dementia; JHMI, Johns Hopkins Medical Institute; M, Male; NINDS, National Institute of Neurological Disease and Stroke; sALS, Sporadic Amyotrophic Lateral Sclerosis; SC-C, Spinal Cord-Cervical; VABBB, VA Biorepository Brain Bank.

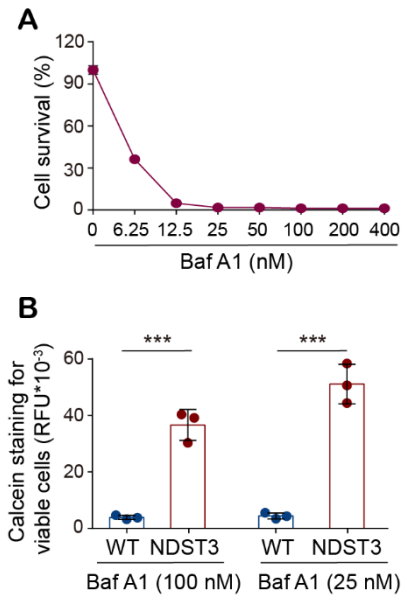

Appendix Figure S1. CRISPR library screening identifies NDST3 as a robust loss-of-function suppressor of bafilomycin A1-induced toxicity (related to Fig 1).

(A) Dose-dependent cytotoxicity was measured using calcein AM staining after 7 days of treatment with various concentrations of bafilomycin A1 (Baf A1) in RPE1 cells (*n* = 3 independent cultures).

(B) Cells edited with a NDST3-targeting sgRNA are identified as being robustly resistant to Baf A1 toxicity at concentration of 100 nM or 25 nM. Cells were treated with Baf A1 for 72 h and measured for cell survival with calcein AM staining (*n* = 3 independent cultures, $^{***}P$ =0.0005 for 100 nM Baf A1, $^{***}P$ =0.0003 for 25 nM Baf A1, two-tailed Student's t-test). Error bars represent ± standard deviation.

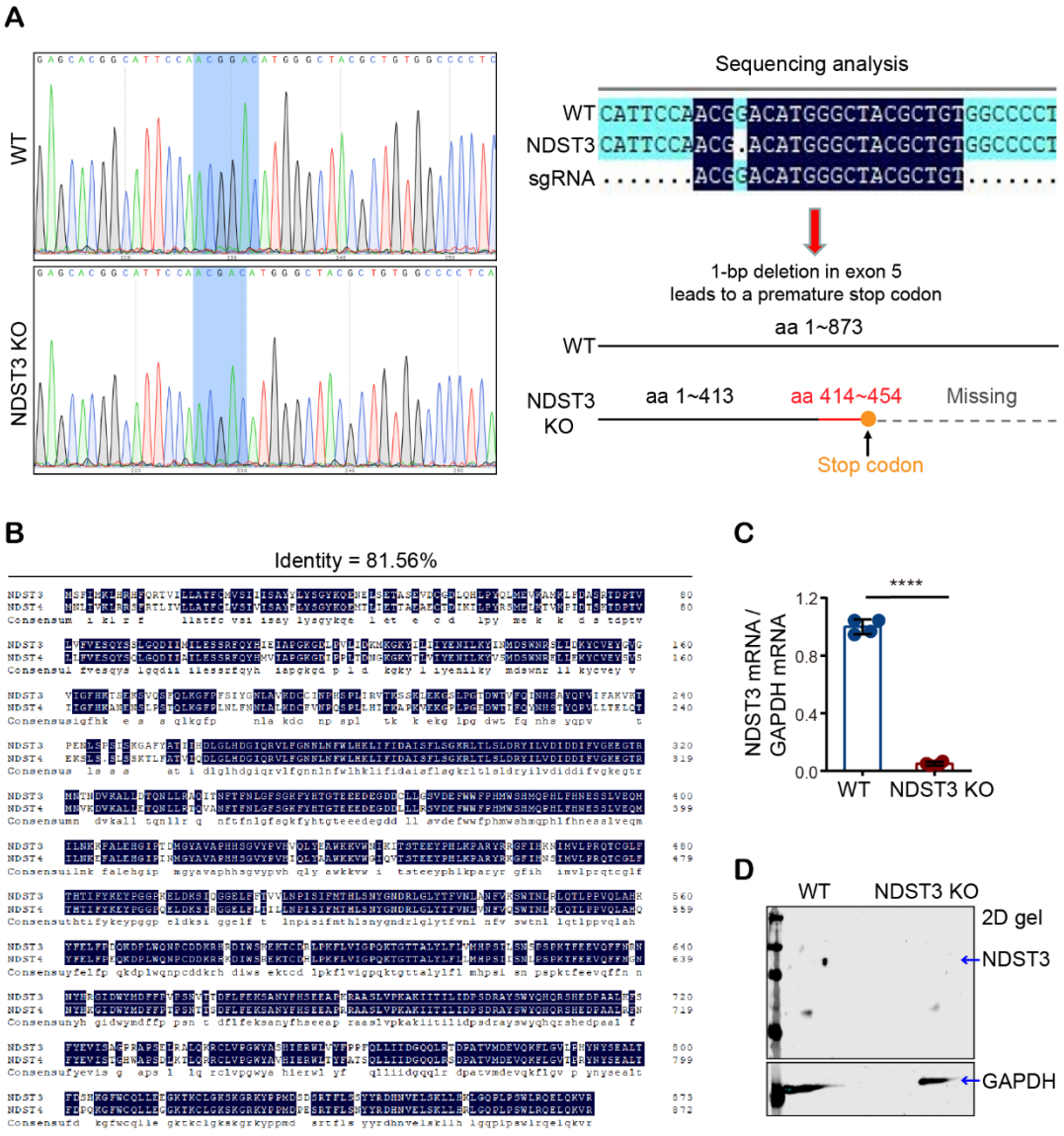

Appendix Figure S2. Verification of the loss of NDST3 in the NDST3 KO RPE1 cell line (related to Fig 1).

(A) The genotype of the NDST3 KO RPE1 cells was analyzed by Sanger sequencing, confirming the 1-bp deletion in exon 5 that creates a premature stop codon.

(B) NDST3 and NDST4 proteins show an amino acid sequence homology of 81.56%.

(C) Quantitative PCR analysis showed a large decrease in NDST3 mRNA in NDST3 KO RPE1 cells when compared to WT cells (n = 4 independent cultures, $^{****}P < 0.0001$, two-tailed Student's t-test). Error bars represent ± standard deviation.

(D) CN/SDS-2D gel electrophoresis shows a complete loss of NDST3 protein in NDST3 KO RPE1 cells.

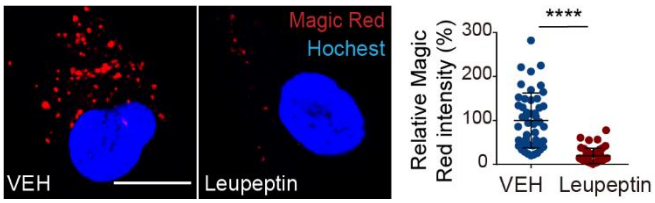

Appendix Figure S3. Validation of the Magic Red assay for measuring Cathepsin B activity (related to Fig 2). RPE1 cells were treated with vehicle (VEH) or leupeptin (0.3 mM, 4h) and then stained with Magic Red (MR)-$(RR)_2$ to measure the Cathepsin B activity. The Magic Red intensity per cell was quantified to represent Cathepsin B activity (n = 48 cells in VEH-treated group, n = 45 cells in Leupeptin-treated group, $^{****}P < 0.0001$, two-tailed Student's t-test). Error bars represent ± standard deviation. Scale bar, 10 μm.

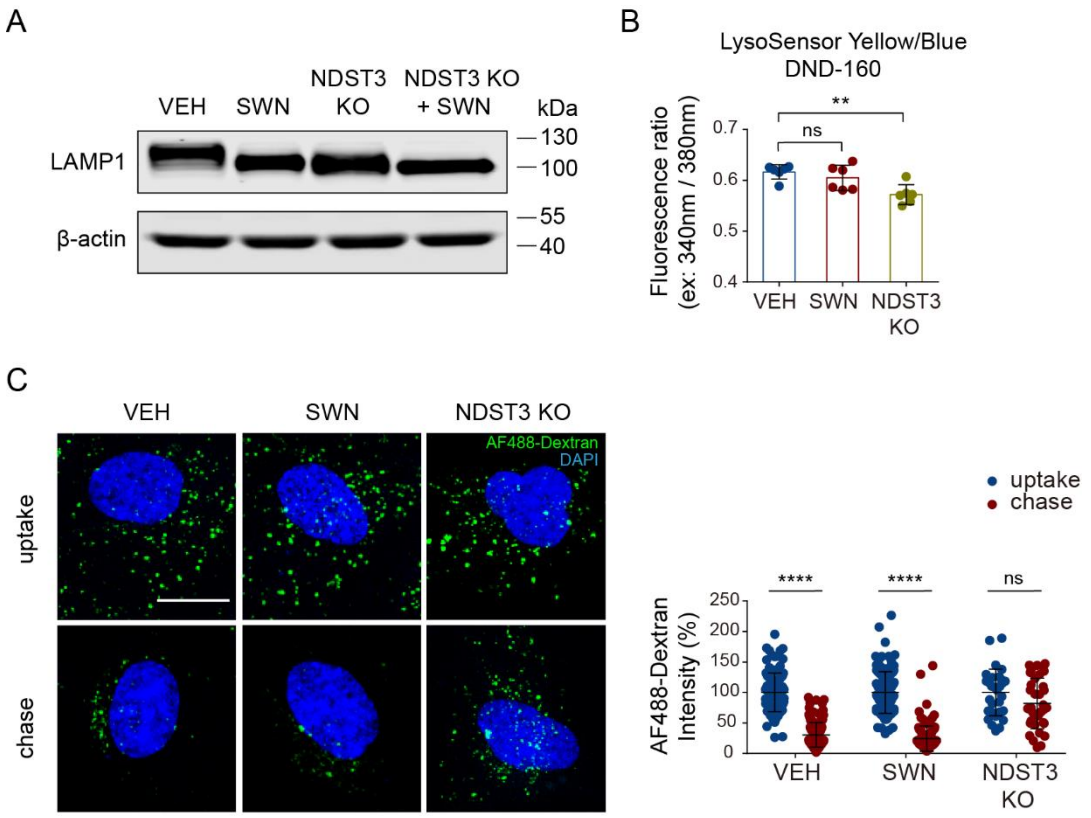

Appendix Figure S4. Inhibition of LAMP1 glycosylation leads to an increase in the migration of LAMP1 on SDS-PAGE but does not affect lysosomal acidification or function (related to Fig 2).

(A) Immunoblotting analysis of LAMP1 from PRE1 cells treated with swainsonine (SWN), a N-linked glycosylation inhibitor, shows that the glycosylation inhibition results in an increase in the migration rate of LAMP1 that comparable to that observed in NDST3 KO RPE1 cells.

(B) Determination of lysosomal pH with a ratiometric probe LysoSensor Yellow/Blue DND-160 shows no impact of glycosylation inhibition on lysosomal acidification. RPE1 cells treated with SWN (25 μg/mL, 48 h) or vehicle (VEH) were stained with LysoSensor Yellow/Blue DND-160 and analyzed for fluorescence signals on a plate reader. NDST3 KO was used as a positive control. The fluorescence ratio of the ratiometric probe was quantified (n = 6 independent cultures, $^{**}P$ = 0.0011, two-tailed Student's t-test).

(C) The Alexa Fluor (AF) 488-dextran degradation assay shows no impact of glycosylation inhibition on lysosomal degradation. RPE1 cells treated with SWN (25 μg/mL, 48 h) or VEH were loaded with 0.4 mg/mL AF488-dextran in culture medium for 20 min, washed, and analyzed for fluorescence signals with or without a 4-h chase period. NDST3 KO was used as a positive control. The AF488 fluorescence intensity per cell was quantified by Fiji software (*n* = 108 cells for VEH-treated uptake group, *n* = 115 cells for SWN-treated uptake group, *n* = 31 cells for NDST3 KO uptake group, *n* = 130 cells for VEH-treated chase group, *n* = 122 cells for SWN-treated chase group, *n* = 36 cells for NDST3 KO chase group $^{****}P < 0.0001$, two-tailed Student's t-test).

Error bars represent ± standard deviation. ns means non-significant. Scale bar, 10 μm.

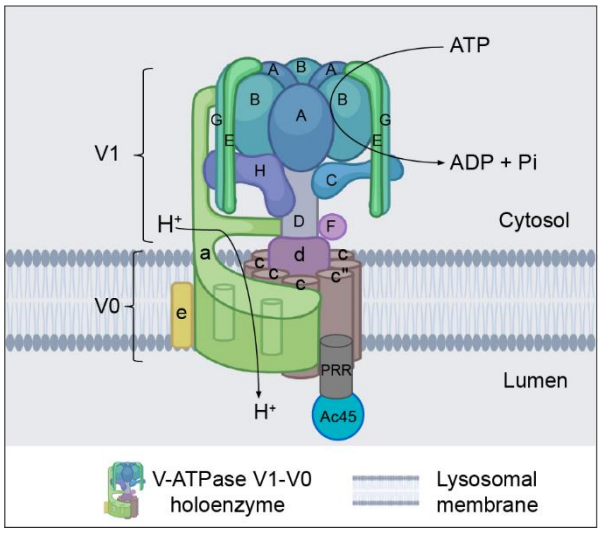

Appendix Figure S5. Schematic representation of the mammalian V-ATPase structure and cellular location (related to Fig 3). The cytosolic V1 domain of V-ATPase is composed of eight subunits, and the integral membrane V0 domain consists of seven subunits. The V1

domain can be reversibly assembled onto V0 to form V-ATPase V1-V0 holoenzymes that have proton pump activity. This figure was created with BioRender.com.

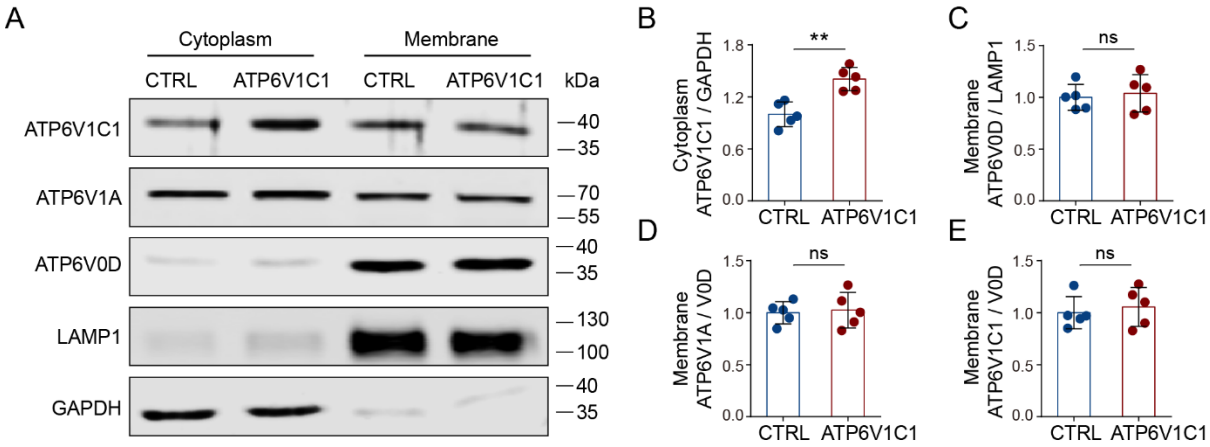

Appendix Figure S6. Overexpression of ATP6V1C1 does not change the level of the V-ATPase V1-V0 holoenzyme (related to Fig 3).

(A) RPE1 cells were transfected with either an ATP6V1C1 ORF plasmid (pLenti6.2-ATP6V1C1-3×FLAG) or a backbone control (CTRL). The cytosolic and membrane fractions were obtained and analyzed by SDS-PAGE and immunoblotting using antibodies against the V-ATPase subunits V1A (ATP6V1A), V1C1 (ATP6V1C1), and V0D (ATP6V0D). LAMP1 and GAPDH were used as loading controls for the membrane and cytosolic fractions, respectively.

(B) Quantification of the cytosolic ATP6V1C1 relative to GAPDH from (**A**) (n = 5 independent experiments, $^{**}P$ = 0.0017, two-tailed Student's t-test).

(C) Quantification of ATP6V0D relative to LAMP1 in the membrane fraction from (**A**) (n = 5 independent experiments, P = 0.7043, two-tailed Student's t-test).

(D, E) The levels of ATP6V1A (**D**) or ATP6V1C1 (**E**) relative to ATP6V0D in the membrane fraction, representing the level of the V-ATPase V1-V0 holoenzyme, were unchanged upon the overexpression of ATP6V1C1 (n = 5 independent experiments, P =0.7900 for **D** and P = 0.6220 for **E**, two-tailed Student's t-test).

Error bars represent ± standard deviation.